Strategies for tuning phonon transport in multilayered structures using a mismatch-based particle model

Nam Q. Le, John C. Duda, Timothy S. English, Patrick E. Hopkins, Thomas E. Beechem et al.

Citation: J. Appl. Phys. **111**, 084310 (2012); doi: 10.1063/1.4704681
View online: http://dx.doi.org/10.1063/1.4704681
View Table of Contents: http://jap.aip.org/resource/1/JAPIAU/v111/i8
Published by the American Institute of Physics.

Strategies for tuning phonon transport in multilayered structures using a mismatch-based particle model

Nam Q. Le,[1,a)] John C. Duda,[1,2] Timothy S. English,[1,2] Patrick E. Hopkins,[1,2] Thomas E. Beechem,[2] and Pamela M. Norris[1]
[1]*Department of Mechanical and Aerospace Engineering, University of Virginia, Charlottesville, Virginia 22904, USA*
[2]*Sandia National Laboratories, Albuquerque, New Mexico 87185, USA*

(Received 10 October 2011; accepted 16 March 2012; published online 20 April 2012)

The performance of many micro- and nanoscale devices depends on the ability to control interfacial thermal transport, which is predominantly mediated by phonons in semiconductor systems. The phonon transmissivity at an interface is therefore a quantity of interest. In this work, an empirical model, termed the thermal mismatch model, is developed to predict transmissivity at ideal interfaces between semiconductor materials, producing an excellent agreement with molecular dynamics simulations of wave packets. To investigate propagation through multilayered structures, this thermal mismatch model is then incorporated into a simulation scheme that represents wave packets as particles, showing a good agreement with a similar scheme that used molecular dynamics simulations as input [P. K. Schelling and S. R. Phillpot, J. Appl. Phys. **93**, 5377 (2003)]. With these techniques validated for both single interfaces and superlattices, they are further used to identify ways to tune the transmissivity of multilayered structures. It is shown that by introducing intermediate layers of certain atomic masses, the total transmissivity can either be systematically enhanced or reduced compared to that of a single interface. Thus, this model can serve as a computationally inexpensive means of developing strategies to control phonon transmissivity in applications that may benefit from either enhancement (e.g., microelectronics) or reduction (e.g., thermoelectrics) in thermal transport. © *2012 American Institute of Physics*.
[http://dx.doi.org/10.1063/1.4704681]

I. INTRODUCTION

Transport mechanisms in micro- and nanostructured materials differ from those in bulk due to the high density of interfaces within them. In particular, superlattice structures have drawn significant attention as a means for controlling electronic and thermal transport. Consequently, many experimental,[1–5] computational,[6–15] analytical,[4,16–27] and empirical[28–34] approaches have sought to investigate the thermal transport across single interfaces and through superlattices. Semiconductor material systems are a primary focus due to their widespread integration in electronic and optical devices. In semiconductors, the majority of thermal energy is carried by phonons, or quantized lattice vibrations. As a result, classical molecular dynamics (MD) simulations are well suited to investigate thermal transport across interfaces within these systems, as the time-evolution of the positions and energies of atoms around an interface can be explicitly monitored.[6–15]

Studies focused on wave-packet dynamics via MD simulations[10–15] have been particularly insightful, since they have allowed for the direct observation of phonon transmission and reflection (scattering) at interfaces between dissimilar materials and at grain boundaries. In these studies, a localized wave packet is constructed from a single branch of the phonon dispersion within a narrow frequency range, which implies a well-defined polarization and wavevector. The positions and velocities of the atoms associated with this wave packet serve as the input to the MD simulation. As the simulation progress, the wave packet propagates towards an interface where it scatters into transmitted and reflected waves. These simulations are performed within an otherwise-stationary crystal, i.e., at 0 K, and thus the total energy of the system can be attributed to the wave packet alone. After the phonon has scattered, the energies of crystals on both sides of the interface, E_1 and E_2, are calculated, and frequency-dependent phonon transmissivity can be described by $\mathscr{T}(\omega) = E_2/(E_1 + E_2)$. In this way, MD simulations can yield great insight into the detailed effects of atomic-level structure on phonon transmissivity, and hence into its effects on thermal transport. However, such simulations can be very complex to implement and computationally expensive. Instead, empirical models are often used to estimate transmissivity with little computational expense, although generally at the expense of the ability to incorporate very detailed atomic structure.

Two empirical models have primarily been employed for predicting phonon transmissivity at interfaces: the acoustic mismatch model (AMM)[28] and the diffuse mismatch model (DMM).[29] The AMM considers the phonon transmission at an interface in the same manner that one would describe the transmission of a sound wave: materials in contact are characterized by acoustic impedances, and those impedances dictate the ratios of energy reflected and transmitted. Consequently, the AMM works best at low temperatures where dominant phonon wavelengths are long and frequencies are low. On the other hand, the DMM assumes

[a)]Electronic mail: nql6u@virginia.edu.

that phonons scatter diffusely, losing memory of their incident polarization and direction. In turn, the probability of a phonon transmitting or reflecting will depend on the mismatch between the phonon density of states and phonon group velocities on either side of the interface. Both of these models have been shown to produce poor agreement with the previously described wave-packet simulations.[14] An approach capable of more accurately predicting phonon transmissivity, while retaining the ease of implementation and negligible computational expense of empirical models, would therefore be useful in the process of thermal design.

In this work, we present a new empirical formulation of phonon transmissivity that differs from those found in the either the AMM or DMM. This formulation, which we will refer to as the thermal mismatch model (TMM), considers the thermal (rather than acoustic) impedances of the materials that compose an interface. The TMM predicts transmissivity in an excellent agreement with the results of previous wave-packet simulations at single interfaces[10] and within multilayered superlattices,[11] suggesting that it can serve as a valuable, computationally inexpensive complement to more robust MD simulations. Hence, we also present several examples in which the TMM is used to investigate strategies to affect the phonon transmissivity in multilayered structures, which can then directly affect thermal transport.

This paper will be organized as follows: in Sec. II, we will develop the TMM and demonstrate its applicability to single ideal (i.e., sharp epitaxial) interfaces. In Sec. III, we will develop a particle model in which the TMM serves as a primary input, further extending the applicability of the TMM to multilayer structures. In Sec. IV, we will apply these tools to investigate novel ways of tuning phonon transmissivity by selection of intermediate layer materials. Section V summarizes the major results of this work.

II. TRANSMISSIVITY ACROSS ISOLATED INTERFACES

In the AMM, the transmissivity at an interface is given as $\mathscr{T} = 4Z_1Z_2/(Z_1+Z_2)^2$, where Z_1 and Z_2 are the acoustic impedances ($Z = \rho v_s$, where ρ is the mass density and v_s is the sound speed) of the materials that compose the interface.[28] This expression is derived by enforcing boundary conditions on displacements and forces at the interface. In its most widely implemented form, the AMM is a continuum model, since it does not consider phonon dispersion. In more recent formulations,[35] some dispersive effects have been taken into account by replacing the sound speed, v_s, with the frequency-dependent phonon group velocity, $v_g(\omega)$, where ω is the phonon angular frequency. In turn, the AMM is capable of providing frequency-dependent phonon transmissivity, although this reformulation does not lead to a substantial agreement with lattice dynamical models or methods, e.g., wave-packet simulations or non-equilibrium Green's functions.[35]

The DMM may also be used to formulate expressions for phonon transmissivity, which depends on assumptions of material isotropy and elastic/inelastic scattering. We assume an isotropic phonon dispersion, which is computationally convenient and shown to yield reasonable agreement with results using the full 3D dispersion.[33] Also, we consider only elastic scattering events that conserve polarization, for consistency with the later formulation via the TMM. In that case, the transmissivity is $\mathscr{T} = k_2(\omega)^2/[k_2(\omega)^2 + k_1(\omega)^2]$, where k_i is the wavenumber (on side i) that corresponds to the phonon frequency ω.[33]

In MD simulations of wave packets scattering from ideal interfaces, it is clear that information about their incident direction is not lost. Therefore, a model describing that phenomenon should be able to capture specular scattering, unlike the DMM. Furthermore, the transmissivity should also depend on temperature as well as frequency; therefore, the distribution function should enter its formulation, unlike in the AMM. As such, we avoid using the acoustic impedance as the central property for defining $\mathscr{T}$, turning instead to the thermal impedance. For a narrow frequency range (as is relevant for wave packets), we define the thermal impedance, I, in units $\mathrm{m^2KW^{-1}s^{-1}}$, as the inverse of the thermal conductance per frequency. Following definitions of thermal conductance as given, for example, in Ref. 36, the thermal impedance is given by

$$I(\omega,T) = \left[\frac{\partial f(\omega,T)}{\partial T} D(\omega)\hbar\omega v_g(\omega)\right]^{-1}, \tag{1}$$

where $f(\omega,T)$ is the Bose–Einstein distribution function, T is the temperature, the quantity $D(\omega) = 1/V \times dN/d\omega$ is the phonon density of states, $\hbar$ is Planck's constant divided by 2π, and $v_g(\omega)$ is the frequency-dependent phonon group velocity.

By describing the thermal impedances of the materials on sides 1 and 2 of the interface in this manner, the frequency-dependent phonon transmissivity, as described by the newly developed TMM, is given by

$$\mathscr{T}(\omega) = \frac{4I_1(\omega,T)I_2(\omega,T)}{(I_1(\omega,T)+I_2(\omega,T))^2}, \tag{2}$$

for phonons at normal angle of incidence, as will be considered in this work for simplicity. Expressions for arbitrary polarization and angle can be obtained readily from analogous formulations in acoustics and optics (for example, see Ref. 37). The form of Eq. (2) is analogous to that of the AMM, insofar as we have assumed that energy approaches the interface in wave form. Implicit in this formulation is the assumption that the two materials abutting the interface are in intimate contact; i.e., adhesion strength is on the order of that within the bulk of each material. In the manner of the AMM, Eq. (2) can be obtained from expressions for transmitted and reflected amplitude ratios, presented in Sec. III, based on the boundary conditions on the wave amplitude at the material interface.

To clarify the interpretation of amplitude, we note that the transmission and reflection of phonons are dictated in the TMM by heat capacities and phonon group velocities (both implicit in thermal impedance, Eq. (1)), as opposed to the mass densities and the sound speeds in the AMM. Strictly speaking, the formulation in terms of thermal

impedance describes energy flux mediated by large populations of phonons, in which case temperatures may be well-defined. In this work, however, we apply the TMM for comparison with wave-packet simulations, in which a localized wave packet consisting of a finite number of phonons travels through a crystal at 0 K. In this case, temperature is ill-defined, and we must consider energy flux to arise directly from the positions and velocities of atoms displaced by a wave packet. Therefore, the amplitude of a wave described in this work which corresponds to the spatial displacement of those atoms, in accordance with the interpretation in wave-packet simulations. This interpretation becomes especially relevant in Sec. III with the introduction of interference effects. This implies that the boundary conditions that give rise to Eq. (2) correspond to the continuity of displacement and force at the interface. At this point, we have thus assumed that energy propagates in the form of mechanical waves and that the transmissivity of these waves at an interface is governed by the thermal impedances of adjacent materials.

Before applying the simplifying assumptions relevant for this work, we point out that the general transmissivity expression retains temperature dependence through the distribution function. This could be relevant, for example, if the expression was applied to the case of inelastic scattering, in which case the distribution function would be evaluated at different frequencies as we have discussed previously.[31,32] However, we have not validated such applications in this work, and the final transmissivity expressions used in this work will be temperature-independent.

With that said, when comparing this model to wave-packet simulations, several conditions lead to significant simplifications of Eqs. (1) and (2). First, we assume that phonons scatter elastically at interfaces, since we intend to compare our results with MD wave-packet simulations in which atomic displacements are small enough to assume harmonic behavior.[10,11] Therefore, incident, transmitted, and reflected wave packets must exist at the same frequency. Second, the normal incidence of the wave packets reduces the problem to the propagation of waves along one dimension, in which case the density of states (per length, per frequency) is expressed as $D(\omega) = 1/L \times dN/d\omega = 1/\pi \times dk/d\omega$. In applications involving a large distribution of phonons, the derivative $dk/d\omega$ is taken as the inverse of the group velocity, v_g^{-1}, reflecting the increase in available states per frequency when the dispersion curve flattens. However, we posit that when modeling elastic scattering of wave packets, only one state (associated with some k_1) dominates the incident wave, and there is only one corresponding state (with another k_2) that is available for the transmitted wave to occupy. Therefore, it is more appropriate to take $L/\pi \times dk/d\omega = dN/d\omega$ as a constant with frequency, rather than varying as the inverse group velocity.

With these assumptions in place for describing wave-packet simulations, Eq. (2) simplifies significantly. After substituting expressions for the thermal impedances I_1 and I_3 based on Eq. (1), only the factor $1/L$ from the density of states and the group velocity v_g remain. Therefore, in these special cases, the transmissivity expression becomes

$$\mathcal{T} = \frac{4\left(\frac{v_{g,1}}{a_1}\right)\left(\frac{v_{g,2}}{a_2}\right)}{\left(\frac{v_{g,1}}{a_1} + \frac{v_{g,2}}{a_2}\right)^2}, \tag{3}$$

where a_i is the lattice parameter of side i, and we have equated the length ratios $L_2/L_1 = a_2/a_1$. We note that Eq. (3) is very similar to the form of Eq. (9) in Ref. 35, which is a form of the AMM with group velocity v_g in place of sound speed v_s. However, an important distinction lies in the absence of atomic masses in Eq. (3); rather than the mass density in the AMM, this equation features the (linear) lattice-point density. This difference is responsible for the elimination of the anomalous transmissivity peak at high frequencies seen in the AMM in Ref. 35 as well as in Fig. 1. That peak is neither predicted by the TMM nor observed in wave-packet simulations.

In order to evaluate the accuracy of phonon transmissivity as predicted by the TMM at an interface between dissimilar materials, we perform example calculations for the [100]-oriented Si/heavy-Si interface studied by Schelling, Phillpot, and Keblinski,[10] where heavy Si is an isotope of Si with an atomic mass 4 times that of Si. In this case, the materials are lattice-matched, so Eq. (3) is further simplified by the cancellation of lattice parameters. Since this model requires knowledge of frequency-dependent group velocities, and hence, phonon dispersion, we first perform harmonic lattice dynamics calculations with the same empirical potentials and parameters as those in the MD study of interest. Thus, we implement the Stillinger–Weber (SW) potential for Si,[38] and we obtain the phonon dispersion along the [100] direction via harmonic lattice dynamics calculations. In this and the following sections, lattice dynamics calculations are performed using the General Utility Lattice Program (GULP).[39] Using the longitudinal group velocities to calculate the thermal impedances in Eq. (2), the resulting frequency-dependent transmissivity is plotted as the red solid line in Fig. 1, demonstrating an excellent agreement

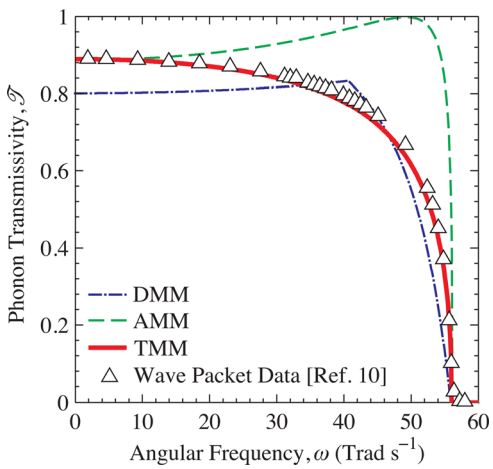

FIG. 1. The frequency-dependent transmissivity $\mathcal{T}$ of a longitudinal phonon traversing a Si/heavy-Si interface. Predictions are plotted based on the DMM with elastic scattering (blue dashed-dotted line), the AMM with phonon dispersion (i.e., when using $v_g(\omega)$ in place of v_s; green dashed line), and the TMM presented in this work (red solid line). Open triangles denote the results of MD wave-packet simulations reported in Ref. 10.

with the results of Ref. 10 for a longitudinal wave packet. This suggests the TMM may serve as a computationally inexpensive substitute for wave-packet simulations at ideal interfaces.

While this model does not take the exact structure of the interface into account—e.g., structural disorder or bonding—it is still useful in cases where the transmissivity is dominated by effects not intrinsic to the interface structure itself. As shown in a wave-packet study of grain boundaries within SW Si,[12] even when significant structural disorder is introduced by a Σ101 twist boundary between grains, transmissivity remains above 90% until packet frequencies increase above 62 Trad s^{-1}. Those strongly affected frequencies correspond to wavelengths shorter than 8 Å, which is approximately the extent of structural disorder. Moreover, in heterogenous semiconductor systems, it has been shown in MD simulations that the predominant effect of cross-species interaction on phonon transport is due to differences in mass, not differences in bond strength.[40]

III. PARTICLE MODEL FOR SUPERLATTICES

In this section, we describe the application of the TMM as the input to a model, similar to the interfering particle model (IPM) of Schelling and Phillpot,[11] in order to investigate the transport of wave packets in superlattices. This model simulates wave packets as localized "particles" with wavelike characteristics as they traverse a superlattice. As explained in that work, the packets can be considered localized particles as long as their dominant wavelength is shorter than their spatial extent (i.e., coherence length), which is in turn smaller than the thicknesses of layers in the structure. This contrasts with approaches that consider coherent phonons propagating throughout the superlattice.[4,16–18] The speed of a packet then corresponds to the group velocity $v = \partial\omega/\partial k$ of phonons at its dominant frequency, based on the dispersion relation obtained as described in Sec. II. The wave aspect of the packets allows them to interfere, in which case their amplitudes, not energies, are superposed. Therefore, it is necessary to determine transmission and reflection coefficients—t and r, respectively—that are ratios of amplitudes, not energies as in Eq. (2). Expressions for these ratios based on impedances are readily available for arbitrary wave polarizations and angles of incidence (see Ref. 37). For simplicity, in this work, we consider phonons approaching only at normal incidence, in which case the different modes of polarization cannot couple with each other at the idealized interface.[18] Then, if a wave packet traveling from materials 1 to 2 is subject to impedances I_1 and I_2 of the form in Eq. (1), the amplitude ratios are given by[37]

$$t_{12} = \frac{2I_1}{I_1 + I_2} \quad \text{and} \quad r_{12} = \frac{I_1 - I_2}{I_1 + I_2}, \tag{4}$$

where frequency dependences have been omitted for brevity. Therefore, wave packets within the structure are characterized by their position, amplitude, wavevector, and velocity. During a given simulation, the elastic assumption implies that all packets have the same frequency, corresponding to different wavevectors and velocities in different regions. Then, for a wave packet n currently in region i, whose amplitude is a fraction a_n of the amplitude of the initial wave packet, its energy is a fraction,

$$\mathscr{T}_n = \frac{I_i}{I_1}|a_n|^2, \tag{5}$$

of the energy of the initial packet (which originated in region 1). It is readily shown that Eqs. (4) and (5) combine to produce Eq. (2) for energy transmissivity at a single interface, in which case transmitted packets simply have an amplitude ratio $a = t_{12}$.

The structure of interest consists of two semi-infinite leads separated by N intermediate layers. Each region is characterized by its thickness and its phonon dispersion relations, which yield frequency-dependent impedances and group velocities. Each interface can then be characterized by transmission and reflection coefficients in both directions as given by Eq. (4), based on the impedances of neighboring regions. In this and the following sections, the frequency-dependent impedance of each region was calculated based on the phonon dispersion of the bulk material, as described in Sec. II. It has been shown elsewhere that the layer thickness of $50a$ is sufficiently large[11] and the 4:1 mass ratio sufficiently small[13] that calculations based on the bulk phonon dispersion yield quantitative agreement with MD wave-packet simulations.

A simulation begins with a single packet in one of the leads propagating toward the superlattice structure. When a packet encounters an interface, it is replaced with two packets—one transmitted, one reflected—with amplitudes according to t and r at that interface. In addition, as wave packets scatter throughout a superlattice, they are combined by adding their amplitudes, if they are spatially coincident (and traveling in the same direction) during a given timestep. Following Ref. 11, packets are deemed spatially coincident when their positions are closer than their dominant wavelengths. The effects of this interference were carefully corroborated in that work using MD simulations for structures up to $N = 4$; the agreement was lost when the model did not allow wave-like interference. Beyond this interference phenomenon, we assume that phonon–phonon scattering can be ignored, since atomic displacements in Ref. 11 are small enough to neglect anharmonic effects. As the simulation proceeds, those packets that travel back into the initial lead are collected as "reflected," while those reaching the far lead are collected as "transmitted." At any time, the energy ratio corresponding to a given packet can be calculated using Eq. (5). We end the simulation when the total energy of all packets within the intermediate layers is less than 0.1% of the energy of the original packet; then, the remainder of the original energy has been either fully reflected or transmitted. Those energies are then used to calculate the total transmissivity $\mathscr{T}$ and reflectivity $\mathscr{R}$.

In order to validate the present model, it is applied to longitudinal wave packets traversing superlattices composed of [100]-oriented layers alternating between Si and heavy Si, with each layer 50 unit cells thick (27.15 nm), thus allowing direct comparison with the results reported by Schelling and Phillpot based on their IPM.[11] That approach is similar to the

one described here, with the primary difference that the amplitude ratios in the IPM (analogous to t and r) were determined using MD wave-packet simulations of single interfaces. The IPM thus offers an advantage over performing computationally expensive MD simulations of structures with many different numbers of layers N. The present approach offers a further advantage by determining transmission and reflection ratios directly by Eq. (4), using impedances calculated according to the TMM, without need for MD simulation of even single interfaces.

The results of simulations are plotted in Fig. 2 for N from 0 to 25 at three different frequencies. Note that the transmissivities converge to nonzero values at large N, a phenomenon due to the wave-like interference of the packets as explained in Ref. 11. These particular superlattices foster constructive interference events due to their uniform layer thickness and special 1:4 mass ratio (corresponding to a 2:1 velocity ratio; see Sec. IV A). Therefore, the transmissivity can be reduced further by modifying the structure to inhibit constructive interference events, as will be shown in Sec. IV B. Finally, note that the transmissivity converges to a slightly larger value for structures with odd N than those with even N at the same phonon frequency, which is an interesting consequence of the interference in these special superlattices. A detailed explanation of this phenomenon is found in Ref. 11.

The agreement with the IPM is good for all three wave packet frequencies, although the discrepancy increases with frequency. For the two lower frequencies (red circles and green squares), transmissivity values differ from those of the IPM by less than 0.01 (i.e., less than 1% of the initial packet energy). This difference reaches nearly 0.03 at the highest frequency, 43.73 Trad s^{-1} (blue diamonds), which is 78% of the cutoff frequency in heavy Si (i.e., the maximum transmitted frequency when considering only elastic scattering). These increased differences are due to the slight underprediction of single-interface transmissivity by the TMM at high frequencies, which is apparent in Fig. 1. This may be due to the onset of anharmonic effects at high frequencies in the MD wave-packet simulations.

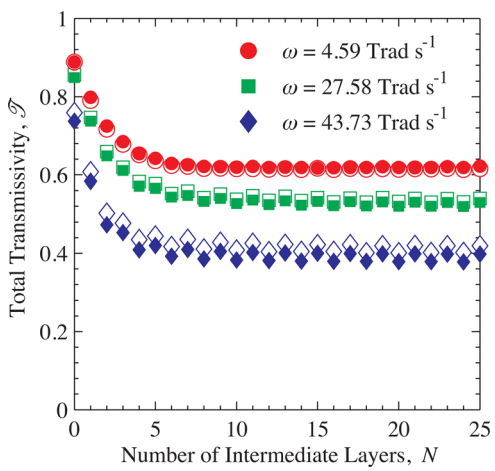

FIG. 2. Total transmissivity of longitudinal wave packets, at three different frequencies, through Si/heavy-Si superlattices with N intermediate layers between semi-infinite leads. Filled markers denote the results of this work, while open markers denote results of the MD-calibrated IPM of Ref. 11. The values of transmissivity with $N=0$ intermediate layers correspond to the values in Fig. 1 for a single interface.

The impact of these discrepancies is mitigated for two reasons. First, the difference is consistent over all values of N rather than compounding with additional layers. Second, such high-frequency phonons make a small contribution to thermal transport. At very low temperatures, those high frequencies are unpopulated ("frozen out"), and even at room temperature Sellan *et al.*[41] found that phonons below 12.6 Trad s^{-1} dominate contributions to the thermal conductivity in bulk SW Si. This corresponds to frequencies for which the TMM demonstrates an excellent agreement. Therefore, these results demonstrate that the TMM can be applied to predict the transmissivity of wave packets through superlattices with accuracy and little computational expense.

IV. STRATEGIES FOR OPTIMIZING TRANSMISSIVITY

The results of Secs. II and III suggest that the TMM can be used to predict phonon transport in a good agreement with more computationally expensive methods. Now, we would like to demonstrate the application of the TMM to gain further insight into how the transmissivity of structures may be tuned by material selection. In Secs. IV A and IV B, we revisit the Si/heavy-Si structures of Sec. III, but now we allow the masses of intermediate layers to be selected between M_{Si} and $4M_{Si}$. Although this is an artificial case, it serves to elucidate the effect of mass as one aspect of controlling transmissivity. First, however, we briefly introduce the concept of impedance matching, which will be useful in interpreting the results throughout this section.

Given two materials with impedances I_1 and I_3, bridged by a material with impedance I_2, the transmissivity is maximized when one chooses

$$I_2 = (I_1 I_3)^{0.5}. \tag{6}$$

That is, transmissivity is maximized when the intermediate impedance is equal to the geometric mean of the neighboring impedances, a result with analogies in acoustics and electrical engineering. This can be understood by observing that the energy of the first transmitted wave packet will always make up the majority of the total transmitted energy, since scattering events cause the amplitudes of reflected packets to shrink geometrically (and their energies are related to the square of the amplitudes). Therefore, according to Eq. (5), the amplitude ratio $a = t_{12}t_{23}$ of that first packet can be used to approximate the total transmissivity as $\mathscr{T} \approx I_3/I_1|t_{12}t_{23}|^2$. Then, applying Eq. (4) for t_{12} and t_{23} and maximizing $\mathscr{T}$ with respect to I_2 yields Eq. (6).

An inductive argument extends this result to the case of multiple intermediate layers. For a structure composed of N layers connecting two semi-infinite leads, $\mathscr{T}$ is maximized when the layers' impedances obey a geometric sequence with $N+2$ terms that begin and end at the impedances of the leads. In other words, impedances of subsequent layers should be related by a common ratio. For example, in the case of $N=1$ layer, the common ratio is $(I_3/I_1)^{0.5}$. As

explained in Sec. II, we consider only elastic scattering, and for simplicity we limit the wave packets to normal incidence.

A. Effect of mass in a single intermediate layer

Consider an $N = 1$ structure as sketched in Fig. 3(a), comprising three regions $i = 1, 2, 3$ that are composed of materials identical to SW Si except in their atomic masses M_i. Regions 1 and 3 form semi-infinite leads with set masses $M_1 = M_{\mathrm{Si}}$ and $M_3 = 4M_{\mathrm{Si}}$, and region 2 forms an intermediate layer with mass M_2. We choose different values of M_2 and, by simulation, determine the fraction of energy $\mathscr{T}$ that is completely transmitted from an incident wave packet at a particular frequency. Simulations were performed for values of M_2/M_1 ranging from 1 to 4 (i.e., from $M_2 = M_1$ to $M_2 = M_3$) in increments of 0.1, and at the same three frequencies considered in Ref. 11, for a total of 93 simulations.

The total transmissivities $\mathscr{T}$ from these simulations are plotted in Fig. 3(b). At the endpoints $M_2/M_1 = 1$ and 4, the structure reduces to a single Si/heavy-Si interface, and the corresponding values of $\mathscr{T}$ for $N = 0$ are recovered. For values in between, overall transmissivity is enhanced since the intermediate value of I_2 reduces mismatch with both neighboring materials. Filled markers indicate the maximum values of $\mathscr{T}$ at the corresponding choices of M_2 for the three different frequencies. The choices of M_2 that maximize $\mathscr{T}$ are approximately $2.0M_{\mathrm{Si}}$, $2.1M_{\mathrm{Si}}$, and $2.3M_{\mathrm{Si}}$ at the frequencies 4.59, 27.58, and 43.73 Trad s^{-1} respectively.

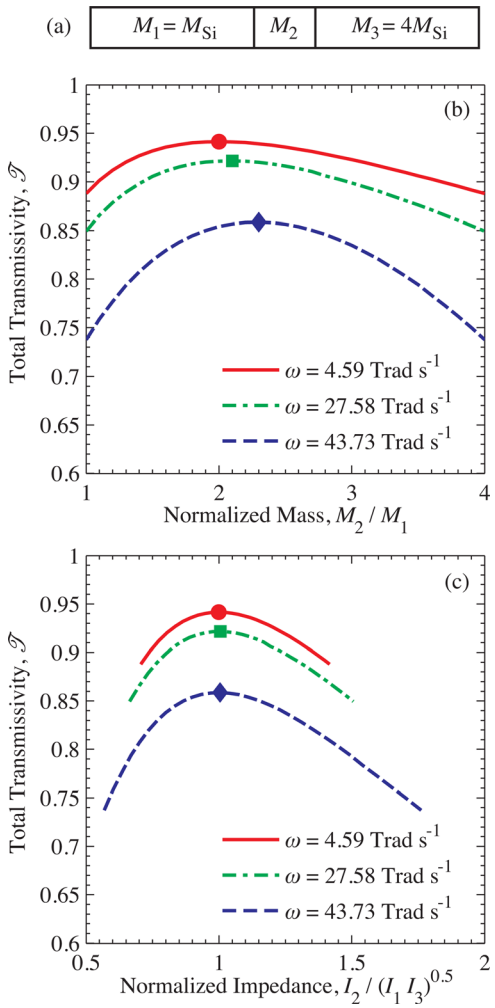

FIG. 3. (a) Sketch of the structure formed from three Si-like materials. Transmission is enhanced when M_2 is chosen between M_1 and M_3. (b) Simulations are performed with different intermediate atomic masses M_2, at the same three frequencies as in Sec. III. Markers denote the maximum value of $\mathscr{T}$ at each frequency; they occur at different choices of M_2. (c) Plot of the same simulations, but for each case, the intermediate impedance I_2 is compared against the calculated impedance $(I_1 I_3)^{0.5}$ that should maximize $\mathscr{T}$. All maximum values of $\mathscr{T}$ occur when $I_2 = (I_1 I_3)^{0.5}$ as expected.

These results can be explained in terms of impedance matching as described earlier. In order to determine the choice of mass M_2 that corresponds to the matched impedance in Eq. (6), we use the result from lattice dynamics[42] that, with all other parameters equal, the phonon dispersion relation in a material i scales with its atomic mass as $\omega_i(k) \propto M_i^{-0.5}$. Since group velocity is given as $v = \partial\omega/\partial k$, this directly implies the simple relationship $v_i(k) = (M_j/M_i)^{0.5} v_j(k)$ between velocities in materials i, j that are identical except in atomic mass. However, we are interested in comparing phonon velocities at the same frequency, not at the same wavevector, and in general $v_i(\omega) \neq (M_j/M_i)^{0.5} v_j(\omega)$ due to dispersive effects. That relation does approach an equality for acoustic phonon modes at the Brillouin zone center, where approximately $\omega \propto k$, which implies $M_2/M_1 \approx (v_1/v_2)^2$ for acoustic phonons at small k. Then, using $I \propto v^{-1}$ from Eq. (1) and applying the impedance-matching constraint of Eq. (6) gives the condition,

$$M_2 \approx (M_1 M_3)^{0.5}, \tag{7}$$

for choosing M_2 to maximize the total transmissivity from materials 1 to 3. Among the three frequencies simulated, the approximation holds best for the lowest frequency, $\omega = 4.59$ Trads^{-1}, which corresponds to a small wavenumber $k = 0.05k_{\mathrm{max}}$ in the longitudinal acoustic branch. Then, Eq. (7) yields $M_2/M_1 \approx (M_{\mathrm{heavySi}}/M_{\mathrm{Si}})^{0.5} = 2$, which corroborates the result in Fig. 3(b) for the lowest frequency (red circle). Again, we note that these low frequencies tend to dominate thermal transport. As frequency increases, dispersive effects become more pronounced, and the optimum value of M_2/M_1 deviates accordingly from Eq. (7) (green square and blue diamond). However, comparing the simulations in terms of impedances rather than mass shows that Eq. (6) is always satisfied at maximum transmissivity, as seen in Fig. 3(c).

B. Effect of mass in multiple intermediate layers

Simulations were also performed to investigate the choices of atomic masses M_i that optimize transmissivity in structures with more than one intermediate layer. For clarity, these simulations were carried out for wave packets only at the low frequency $\omega = 4.59$ Trad s^{-1} so that approximations analogous to Eq. (7) can be used. In that case, a given relationship between masses M_i implies an equivalent relationship between impedances I_i. One set of simulations was performed with $N = 2$, and another set with $N = 4$. Each intermediate mass is again chosen such that M_i/M_1 ranges from 1 to 4 in increments of 0.1, and a simulation is performed for each set of M_i, resulting in 961 simulations with

TABLE I. Descriptions of five selected $N = 2$ structures, along with the transmissivity $\mathscr{T}$ resulting from each simulation for the low frequency $\omega = 4.59$ Trad s^{-1} only. Structures are listed in order of descending $\mathscr{T}$. Atomic masses M_i are given in units of $M_1 = M_{Si}$. In this case, the maximum mass mismatch (and hence the maximum impedance mismatch) yields the smallest value of $\mathscr{T}$.

Label	Description	M_1	M_2	M_3	M_4	$\mathscr{T}$
2A	Smooth, geometric	1.0	1.6	2.5	4.0	0.961
2B	Smooth, linear	1.0	2.0	3.0	4.0	0.956
2C	Smooth, opposite concavity	1.0	2.5	3.4	4.0	0.942
2D	Single interface	1.0	1.0	4.0	4.0	0.888
2E	Zigzag, maximum mismatch	1.0	4.0	1.0	4.0	0.752

$N = 2$ and 923 521 simulations with $N = 4$. From these simulations, we can identify the patterns of M_i that tend to maximize and minimize $\mathscr{T}$. In addition, the results reveal the extent to which the transmissivity $\mathscr{T}$ is sensitive to deviations from the optimum choices of M_i.

Eleven of these simulations—five with $N = 2$, six with $N = 4$—have been selected for presentation in Tables I and II, which list for each simulation the particular sequence of M_i of the regions i and the resulting transmissivity $\mathscr{T}$. The following discussion explains the verbal descriptions given in the table, which serve to distinguish the mass sequences qualitatively. For each value of N, a structure is shown that reproduces the single-interface case as a basis for comparison (type D structures); these both produce $\mathscr{T} = 0.88800$ in agreement with Fig. 1. From there, transmissivity can be either enhanced (types A, B, and C) or reduced (types E and F) depending on the choices of M_i.

Choosing a strictly monotonic ("smooth") sequence of M_i that connects M_1 to M_{N+2} tends to enhance the transmissivity, since impedance mismatch is reduced. Among the simulations performed, the transmissivity was maximized when the masses M_i were closest to following a geometric series from M_{Si} to $4M_{Si}$. Due to the low frequency, Eq. (7) holds, and these choices of M_i correspond to a geometric sequence of impedances as well, in agreement with the arguments at the beginning of this section. For example, for $N = 2$, the normalized masses in structure 2 A correspond to the geometric sequence $(4^{0/3}, 4^{1/3}, 4^{2/3}, 4^{3/3})$, yielding a transmissivity $\mathscr{T} = 0.961$ that is significantly higher than for the single interface.

In addition, we observe that the value of $\mathscr{T}$ is relatively insensitive to small deviations from the optimum choices of M_i. For each value of N, two other smooth sequences of M_i are shown in addition to the optimum case; one sequence is linear (type B structures), and the other exhibits the same curvature as the optimum case, but with opposite concavity (type C). The transmissivities resulting from these simulations are only slightly lower than those of the optimum cases, demonstrating that the enhancement in $\mathscr{T}$ is not sensitive to small departures from the optimum impedance-matched structure.

TABLE II. Same as Table I, but for six selected $N = 4$ structures. Note that although structure 4E (an *AB* superlattice) exhibits the sequence of greatest impedance mismatch, it does not exhibit the minimum transmissivity because of constructive interference.

Label	Description	M_1	M_2	M_3	M_4	M_5	M_6	$\mathscr{T}$
4A	Smooth, geometric	1.0	1.3	1.7	2.3	3.0	4.0	0.976
4B	Smooth, linear	1.0	1.6	2.2	2.8	3.4	4.0	0.973
4C	Smooth, opposite concavity	1.0	2.0	2.7	3.3	3.7	4.0	0.961
4D	Single interface	1.0	1.0	1.0	4.0	4.0	4.0	0.888
4E	Zigzag, maximum mismatch	1.0	4.0	1.0	4.0	1.0	4.0	0.654
4F	Zigzag, minimum $\mathscr{T}$	1.0	3.9	1.0	4.0	1.0	4.0	0.623

On the other hand, the total transmissivity can also be reduced relative to the single interface by inserting layers with masses M_i that alternately increase and decrease ("zigzag"). One might expect that the minimum $\mathscr{T}$ would occur when the atomic masses M_i alternate between the limits M_{Si} and $4M_{Si}$ (type E structures), since that sequence creates the greatest impedance mismatch between adjacent layers. This is true among the $N = 2$ structures, in which case the structure 2E yielded the smallest transmissivity. However, this is not the case for higher values of N. Among the simulations with $N = 4$ layers, 178 yielded transmissivities that were lower than that of structure 4E. This is because that sequence forms a perfect Si/heavy-Si superlattice that facilitates constructive interference events, as described in Sec. III. Thus, an incidental enhancement due to constructive interference counteracts the reduction due to impedance mismatch. The minimum transmissivity actually occurred in the structure 4F, since it exhibits nearly the maximum impedance mismatch, while the small deviation in M_2 disrupts any constructive interference.

Therefore, we observe that a perfect *AB* superlattice does exhibit reduced transmissivity compared to the single *AB* interface, but if constructive interference occurs, then even lower transmissivities can be obtained from slightly "imperfect" superlattices. We have demonstrated that this can be achieved by slight variations in atomic mass, but it can also be achieved by other means. For example, Schelling and Phillpot[11] demonstrated similar reductions by introducing random deviations of up to 10% in the thicknesses of all layers in a superlattice. To draw a more direct analogy with structure 4F, we simulate another $N = 4$, Si/heavy-Si superlattice with modification to region 2 only. Adjusting the thickness of only that layer from 50 to 48 unit cells (27.15 to 26.06 nm) yields a transmissivity of $\mathscr{T} = 0.624$, which is approximately the same reduction observed for the mass-adjusted structure 4F.

V. SUMMARY

We have presented the TMM to predict the frequency-dependent phonon transmissivity at ideal interfaces based on the thermal impedances of the adjacent materials. Specifically, the results of this work have validated Eq. (3) for predicting transmissivity in the special case of wave packet simulations of elastic scattering at normal incidence. However, we emphasize that further verification would be necessary in order to evaluate the validity of Eqs. (1) and (2) when applied to more general cases. The transmissivities predicted by the TMM were found in a good agreement with those reported from MD wave-packet simulations of an Si/heavy-Si interface, as well as those reported by the IPM for

Si/heavy-Si superlattices. We note that, although only cases of longitudinal polarization have been presented here, similar agreement can also be obtained with the transmissivities reported in Ref. 14 for transverse wave packets at a Ar/Kr interface. Therefore, the TMM is a computationally inexpensive tool for investigating phonon transmissivity in complex structures, and it can be used to reveal novel trends over broad parameter spaces, as presented in Sec. IV B when freely selecting the atomic masses of four intermediate layers. Examples were presented in which the insertion of intermediate layers either enhanced or reduced transmissivity in a nontrivial but predictable way. Trends such as those may lead to thermal management strategies relevant to engineering applications, since the phonon transmissivity enters directly into expressions of practical quantities like the thermal boundary resistance.[36]

ACKNOWLEDGMENTS

The authors at U.Va. acknowledge the financial support of the Air Force Office of Scientific Research (Grant No. FA9550-09-1-0245). N.Q.L. acknowledges support from the U.Va. Office of the Vice President for Research. J.C.D. and T.S.E. are appreciative of funding from the National Science Foundation through the Graduate Research Fellowship Program. T.S.E. is appreciative of support by the Department of Defense through the National Defense Science & Engineering Graduate Fellowship. The authors from Sandia are appreciative of funding from the LDRD program office. Sandia is a multiprogram laboratory operated by Sandia Corporation, a wholly owned subsidiary of Lockheed Martin Corporation, for the United States Department of Energy's National Nuclear Security Administration under Contract No. DE-AC04-94AL85000. The authors would also like to thank C. H. Baker, C. B. Saltonstall, and M. R. Sinden-Redding for valuable discussions.

[1]W. S. Capinski and H. J. Maris, Physica B **219–220**, 699 (1996).
[2]S.-M. Lee, D. G. Cahill, and R. Venkatasubramanian, Appl. Phys. Lett. **70**, 2957 (1997).
[3]D. G. Cahill, Rev. Sci. Instrum. **75**, 5119 (2004).
[4]Y. Ezzahri, S. Grauby, J. M. Rampnoux, H. Michel, G. Pernot, W. Claeys, S. Dilhaire, C. Rossignol, G. Zeng, and A. Shakouri, Phys. Rev. B **75**, 195309 (2007).
[5]P. M. Norris and P. E. Hopkins, J. Heat Transfer **131**, 043207 (2009).
[6]R. J. Stevens, L. V. Zhigilei, and P. M. Norris, Int. J. Heat Mass Transfer **50**, 3977 (2007).
[7]E. S. Landry, M. I. Hussein, and A. J. H. McGaughey, Phys. Rev. B **77**, 184302 (2008).
[8]E. S. Landry and A. J. H. McGaughey, Phys. Rev. B **80**, 165304 (2009).
[9]E. S. Landry and A. J. H. McGaughey, Phys. Rev. B **79**, 075316 (2009).
[10]P. K. Schelling, S. R. Phillpot, and P. Keblinski, Appl. Phys. Lett. **80**, 2484 (2002).
[11]P. K. Schelling and S. R. Phillpot, J. Appl. Phys. **93**, 5377 (2003).
[12]P. K. Schelling, S. R. Phillpot, and P. Keblinski, J. Appl. Phys. **95**, 6082 (2004).
[13]Z. T. Tian, B. E. White, Jr., and Y. Sun, Appl. Phys. Lett. **96**, 263113 (2010).
[14]N. A. Roberts and D. G. Walker, J. Appl. Phys. **108**, 123515 (2010).
[15]L. Sun and J. Y. Murthy, J. Heat Transfer **132**, 102403 (2010).
[16]V. Narayanamurti, H. L. Störmer, M. A. Chin, A. C. Gossard, and W. Wiegmann, Phys. Rev. Lett. **43**, 2012 (1979).
[17]S. Y. Ren and J. D. Dow, Phys. Rev. B **25**, 3750 (1982).
[18]S. Tamura, D. H. Hurley, and J. P. Wolfe, Phys. Rev. B **38**, 1427 (1988).
[19]D. A. Young and H. J. Maris, Phys. Rev. B **40**, 3685 (1989).
[20]G. Chen and M. Neagu, Appl. Phys. Lett. **71**, 2761 (1997).
[21]G. Chen, Phys. Rev. B **57**, 14958 (1998).
[22]G. Chen, J. Heat Transfer **121**, 945 (1999).
[23]G. Chen and T. Zeng, Microscale Thermophys. Eng. **5**, 71 (2001).
[24]H. Zhao and J. B. Freund, J. Appl. Phys. **97**, 024903 (2005).
[25]H. Zhao and J. B. Freund, J. Appl. Phys. **105**, 013515 (2009).
[26]F. X. Alvarez, J. Alvarez-Quintana, D. Jou, and J. Rodriguez Viejo, J. Appl. Phys. **107**, 084303 (2010).
[27]S. P. Hepplestone and G. P. Srivastava, Phys. Rev. B **82**, 144303 (2010).
[28]W. A. Little, Can. J. Phys. **37**, 334 (1959).
[29]E. T. Swartz and R. O. Pohl, Rev. Mod. Phys. **61**, 605 (1989).
[30]T. Beechem, S. Graham, P. E. Hopkins, and P. M. Norris, Appl. Phys. Lett. **90**, 054104 (2007).
[31]P. E. Hopkins, J. Appl. Phys. **106**, 013528 (2009).
[32]P. E. Hopkins, J. C. Duda, and P. M. Norris, J. Heat Transfer **133**, 062401 (2011).
[33]J. C. Duda, T. E. Beechem, J. L. Smoyer, P. M. Norris, and P. E. Hopkins, J. Appl. Phys. **108**, 073515 (2010).
[34]G. C. Loh, B. K. Tay, and E. H. T. Teo, Appl. Phys. Lett. **97**, 121917 (2010).
[35]P. E. Hopkins, P. M. Norris, M. S. Tsegaye, and A. W. Ghosh, J. Appl. Phys. **106**, 063503 (2009).
[36]G. Chen, *Nanoscale Energy Transport and Conversion: A Parallel Treatment of Electrons, Molecules, Phonons, and Photons* (Oxford University Press, New York, NY, 2005).
[37]B. A. Auld, *Acoustic Fields and Waves in Solids* (John Wiley & Sons, New York, NY, 1973).
[38]F. H. Stillinger and T. A. Weber, Phys. Rev. B **31**, 5262 (1985).
[39]J. D. Gale and A. L. Rohl, Mol. Simul. **29**, 291 (2003).
[40]A. Skye and P. K. Schelling, J. Appl. Phys. **103**, 113524 (2008).
[41]D. P. Sellan, J. E. Turney, A. J. H. McGaughey, and C. H. Amon, J. Appl. Phys. **108**, 113524 (2010).
[42]M. T. Dove, *Introduction to Lattice Dynamics, Cambridge Topics in Mineral Physics and Chemistry No. 4* (Cambridge University Press, Cambridge, England, 1993).